

## Examination of a critical roughness height for outer layer similarity

K. A. Flack

*Department of Mechanical Engineering, United States Naval Academy, Annapolis, Maryland 21402, USA*

M. P. Schultz and J. S. Connelly

*Department of Naval Architecture and Ocean Engineering, United States Naval Academy, Annapolis, Maryland 21402, USA*

(Received 1 May 2007; accepted 6 June 2007; published online 19 September 2007)

The existence of a critical roughness height for outer layer similarity between smooth and rough wall turbulent boundary layers is investigated. Results are presented for boundary layer measurements on flat plates covered with sandgrain and woven mesh with the ratio of the boundary layer thickness to roughness height ( $\delta/k$ ) varying from 16 to 110 at  $Re_\theta = 7.3 \times 10^3 - 13 \times 10^3$ . In all cases tested, the layer directly modified by the roughness (the roughness sublayer) is confined to a region  $<5k$  or  $<3k_s$  from the wall (where  $k_s$  is the equivalent sandgrain roughness height). In the larger roughness cases, this region of turbulence modification extends into the outer flow. However, beyond  $5k$  or  $3k_s$  from the wall, similarity in the turbulence quantities is observed between the smooth and rough wall boundary layers. These results indicate that a critical roughness height, where the roughness begins to affect most or all of the boundary layer, does not exist. Instead, the outer flow is only gradually modified with increasing roughness height as the roughness sublayer begins to occupy an ever increasing fraction of the outer layer. [DOI: 10.1063/1.2757708]

### I. INTRODUCTION

Smooth wall studies have provided the basis for understanding rough wall flows, with engineering models generally treating surface roughness as a small perturbation to the smooth wall boundary layer. However, questions remain as to the extent of the roughness-induced perturbation and whether or not smooth wall boundary layer theory is valid for large roughness. A fundamental question with implications for the use of wall models and large eddy simulations for the computation of rough wall flows is if the buffer layer can be perturbed or destroyed without transmitting anything to the outer flow except a change in skin friction.<sup>1</sup> If so, what happens for larger roughness elements?

The major effect of roughness on the mean velocity profile plotted in inner variables is a downward shift in the log-law region ( $\Delta U^+$ ), termed the roughness function, while the shape of the profile in the outer layer is unchanged.<sup>2</sup> In outer scaling, this results in the collapse of smooth and rough profiles in velocity-defect form, which is supported by numerous studies.<sup>3-8</sup> This mean flow similarity indicates that the use of wall functions for rough wall boundary layer models may be appropriate. However, results from Krogstad *et al.*<sup>9</sup> and Keirsbulck *et al.*<sup>10</sup> indicate that the wake strength of the mean velocity profile is increased on rough walls, implying the effect of surface roughness may propagate well into the outer region. If this is the case, application of rough wall models that rely on outer layer similarity will yield erroneous results.

Townsend's<sup>11</sup> Reynolds number similarity hypothesis and subsequent extensions by Perry and Chong<sup>12</sup> and Raupach *et al.*<sup>4</sup> state that the turbulent stresses are independent of surface condition outside the roughness sublayer (or viscous sublayer in the smooth wall case) at sufficiently high

Reynolds number when normalized by the wall shear stress. That is, the turbulence in the outer layer is unaffected by surface roughness except in the role it plays in modifying the outer velocity and length scales. The underlying assumption of Townsend's hypothesis is that the boundary layer thickness ( $\delta$ ) is large compared to the roughness height ( $k$ ). The roughness sublayer is typically thought to extend  $\sim 5$  roughness heights from the wall.<sup>4</sup> A number of studies have shown support for Townsend's hypothesis for three-dimensional roughness including the works of Ligrani and Moffat<sup>13</sup> for packed spheres, Perry and Li<sup>14</sup> for expanded mesh, Kunkel and Marusic<sup>15</sup> for salt flats ground cover, Shockling *et al.*<sup>16</sup> for a honed pipe, and the present authors for sanded surfaces,<sup>6</sup> packed spheres with and without grit,<sup>7</sup> and sandpaper and woven mesh.<sup>8</sup> Recently, the present authors<sup>17</sup> also demonstrated support for the hypothesis for the limiting case of fully rough flow at high Reynolds number for a roughness that is a very small fraction of the boundary layer thickness.

In contrast, changes to the Reynolds stresses over a large portion of the outer layer have been observed for flows over woven mesh and transverse bar roughness in the experimental work of Krogstad and Antonia,<sup>18</sup> Tachie *et al.*,<sup>19</sup> and Keirsbulck *et al.*<sup>10</sup> Recent numerical simulations of turbulent channel flow<sup>20,21</sup> have also shown roughness effects extending into the outer layer. A possible explanation for the disparate findings may be due to the "strong" roughness used in the investigations, where effects were observed in the outer layer. A strong roughness can be thought of as a surface whose roughness height (or alternatively equivalent sandgrain roughness height<sup>22</sup>) is a significant portion of the inner layer thickness,<sup>7</sup> but just how significant a portion is unclear. Therefore, the maximum roughness height for which outer layer similarity may be assumed to be valid needs to be defined. For cases with larger roughness than this, the clas-

# Report Documentation Page

Form Approved  
OMB No. 0704-0188

Public reporting burden for the collection of information is estimated to average 1 hour per response, including the time for reviewing instructions, searching existing data sources, gathering and maintaining the data needed, and completing and reviewing the collection of information. Send comments regarding this burden estimate or any other aspect of this collection of information, including suggestions for reducing this burden, to Washington Headquarters Services, Directorate for Information Operations and Reports, 1215 Jefferson Davis Highway, Suite 1204, Arlington VA 22202-4302. Respondents should be aware that notwithstanding any other provision of law, no person shall be subject to a penalty for failing to comply with a collection of information if it does not display a currently valid OMB control number.

1. REPORT DATE <b>MAY 2007</b>		2. REPORT TYPE		3. DATES COVERED <b>00-00-2007 to 00-00-2007</b>	
4. TITLE AND SUBTITLE <b>Examination of a critical roughness height for outer layer similarity</b>				5a. CONTRACT NUMBER	
				5b. GRANT NUMBER	
				5c. PROGRAM ELEMENT NUMBER	
6. AUTHOR(S)				5d. PROJECT NUMBER	
				5e. TASK NUMBER	
				5f. WORK UNIT NUMBER	
7. PERFORMING ORGANIZATION NAME(S) AND ADDRESS(ES) <b>United States Naval Academy, Department of Mechanical Engineering, Annapolis, MD, 21402</b>				8. PERFORMING ORGANIZATION REPORT NUMBER	
9. SPONSORING/MONITORING AGENCY NAME(S) AND ADDRESS(ES)				10. SPONSOR/MONITOR'S ACRONYM(S)	
				11. SPONSOR/MONITOR'S REPORT NUMBER(S)	
12. DISTRIBUTION/AVAILABILITY STATEMENT <b>Approved for public release; distribution unlimited</b>					
13. SUPPLEMENTARY NOTES					
14. ABSTRACT					
15. SUBJECT TERMS					
16. SECURITY CLASSIFICATION OF:			17. LIMITATION OF ABSTRACT	18. NUMBER OF PAGES	19a. NAME OF RESPONSIBLE PERSON
a. REPORT <b>unclassified</b>	b. ABSTRACT <b>unclassified</b>	c. THIS PAGE <b>unclassified</b>			

sical concept of the roughness being a small perturbation to the smooth wall boundary layer, with its effect characterized solely by  $\Delta U^+$ , must be abandoned. Based upon his review, Jiménez<sup>1</sup> suggested that similarity in the outer flow can be expected for rough wall flows with  $\delta/k$  as a minimum greater than 40, but likely the limiting value is closer to 80. Recently, Schultz and Flack<sup>7</sup> and Flack *et al.*<sup>8</sup> have observed similarity for roughness with  $\delta/k$  of 29 and 45, respectively. The proper roughness length scale will likely be more than simply a measure of the roughness height to boundary layer thickness, but moreover will include the effects of the roughness type and density on the mean and turbulent flow. Using the equivalent sandgrain roughness as a roughness scale does provide a common currency<sup>23</sup> for a variety of roughness types, since it incorporates the effect of the surface roughness on the mean flow. However, it may not be the best indicator of effects on the Reynolds stresses and higher order moments, and has the disadvantage of not being known for a generic roughness *a priori*.

The goal of the present research is to document the effect of increasing roughness height on the outer layer turbulence statistics in fully developed turbulent boundary layers on two types of three-dimensional roughness. The range of  $\delta/k$  was  $16 \leq \delta/k \leq 110$  ( $6 \leq \delta/k_s \leq 91$ ) in the study. This range spans from where outer layer similarity is expected to be valid to significantly rougher surfaces, where similarity is expected to fail based on the criteria of Jiménez.<sup>1</sup> From these results, the similarity of both the mean velocity and turbulence structure on rough and smooth walls is critically evaluated. Additionally, the limiting roughness height where outer layer similarity holds is explored.

## II. EXPERIMENTAL FACILITIES AND METHODS

The experiments were conducted in the U.S. Naval Academy's large recirculating water tunnel. The test section is  $40 \times 40$  cm<sup>2</sup> in cross section and is 1.8 m in length, with a tunnel velocity range of 0–8.0 m/s and a freestream turbulence intensity of  $\sim 0.5\%$ . The present tests were run at a tunnel speed of  $\sim 2.0$  m/s ( $Re_x = 2.7 \times 10^6$ ,  $Re_\theta = 6.1 \times 10^3 - 13 \times 10^3$ ). The test plates were flush mounted into a splitter-plate test fixture. The test fixture was mounted horizontally, at mid-depth in the tunnel. The first 200 mm of the test fixture is covered with #36-grit sandpaper to ensure adequate turbulent boundary layer tripping. Measurements were obtained 1.35 m downstream of the trip, allowing for a sufficient boundary layer growth. The upper, removable wall of the tunnel is adjustable to account for boundary layer growth, producing a nearly zero pressure gradient boundary layer, with an acceleration parameter of  $K \leq 1 \times 10^{-8}$ , where  $K$  is defined as

$$K = \frac{v}{U_e^2} \frac{dU_e}{dx}. \quad (1)$$

A plan view schematic of the facility is shown in Fig. 1. Additional details of the experimental facility can be found in Schultz and Flack<sup>6</sup> and Flack *et al.*<sup>8</sup>

Seven surfaces were tested in this study, as listed in Table I: one was a smooth cast acrylic surface; the other six

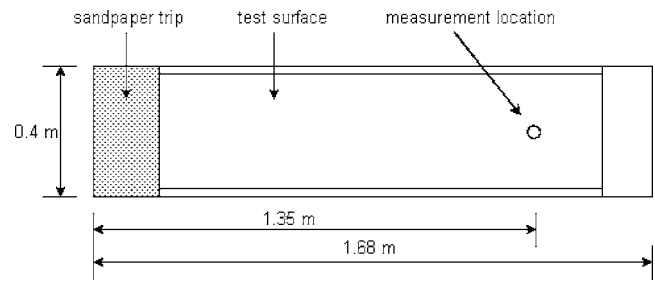


FIG. 1. Schematic of flat plate test fixture.

were rough surfaces. Three surfaces were covered with wet/dry sandpaper. These included 80-, 24-, and 12-grit sandpaper. The remaining three were covered with woven wire mesh with pitch to diameter ratios of 6.25 for M1, 4.58 for M2, and 8.45 for M3. The roughness height,  $k$ , given in Table I is the maximum peak to trough height measured over a  $50 \times 50$  mm<sup>2</sup> sampling area. For the sandpaper surfaces, this was measured using a dial indicator. For the mesh surfaces, it was taken to be twice the wire diameter. The correct scale to use to accurately characterize the roughness height is still an active area of research and may depend on additional parameters to account for differences in texture.

Velocity measurements were made using a TSI FSA3500 two-component, fiber-optic laser Doppler velocimeter (LDV). The LDV consists of a four-beam fiber-optic probe that collects data in backscatter mode. A custom designed beam displacer was added to the probe to shift one of the four beams, resulting in three coplanar beams that can be aligned parallel to the wall. This allowed for near-wall measurements without having to tilt the probe at a small angle or rotate the probe to resolve velocity components. The measurement volume diameter was  $90 \mu\text{m}$  and its length was 1.3 mm. The viscous length scale ( $\nu/u_\tau$ ) varied from  $7.5 \mu\text{m}$  for the roughest surface to  $13 \mu\text{m}$  for the smooth wall. The diameter of the probe volume, therefore, ranged from 7 to 13 viscous lengths in the present study. The flow was seeded with  $2 \mu\text{m}$  alumina particles. The seed volume was controlled to achieve acceptable data rates while maintaining a low burst density signal.<sup>24</sup> A total of 40 000 random velocity samples were obtained in coincidence mode at each location in the boundary layer. Doppler bursts for the two channels were required to fall within a  $50\text{-}\mu\text{s}$  coincidence window or the sample was rejected. The probe was traversed to approximately 40 locations within the boundary layer with a Velmex three-axis traverse unit. The traverse allowed the position of the probe to be maintained to  $\pm 5 \mu\text{m}$  in all directions.

Precision uncertainty estimates for the velocity measurements were made through repeatability tests using the procedure given by Moffat.<sup>25</sup> Ten replicate velocity profiles were taken on both a smooth and a rough plate. LDV measurements are susceptible to a variety of bias errors including angle, velocity, and velocity gradient biases, as detailed by Edwards.<sup>26</sup> Fringe bias results from the inability to sample scattering particles passing through the measurement volume at large angles since several fringe crossings are needed to validate a measurement. In this experiment, the fringe bias was considered insignificant, as the beams were shifted well

TABLE I. Experimental test conditions.

Surface	Symbol	$U_e$ (m/s)	$Re_\theta$	Wall offset (mm)	$u_\tau$ Clauser (m/s)	$u_\tau$ TS (m/s)	$\Delta U^+$	$\delta$ (mm)	$\delta^+$	$\delta^*$ (mm)	$\theta$ (mm)	$k$ (mm)	$k^+$	$k_s^+$	$\delta/k$	$\delta/k_s$
Smooth		2.00	6140		0.0763	0.0746		32.5	2480	4.05	3.08					
80-grit sandpaper	S1	1.98	7970	0.175	0.0917	0.0901	5.24	37.2	3250	5.93	4.22	0.690	60	36	54	91
Fine mesh	M1	1.99	7290	0.130	0.0981	0.0951	6.31	34.8	3080	5.83	4.06	0.320	28	56	110	55
24-grit sandpaper	S2	1.99	8970	0.580	0.120	0.119	10.8	37.9	4140	7.91	4.96	1.80	200	360	21	11
Medium mesh	M2	2.00	9110	0.400	0.119	0.113	10.9	38.3	4180	8.00	5.00	1.40	150	370	27	11
12-grit sandpaper	S3	2.00	12 430	1.130	0.132	0.131	13.0	44.9	6060	9.99	6.08	2.85	380	860	16	7.0
Coarse mesh	M3	2.00	13 050	0.810	0.133	0.126	13.7	46.8	6350	10.91	6.40	2.45	330	1150	19	5.5

above a burst frequency representative of twice the freestream velocity. Validation bias results from filtering too near the signal frequency and any processor biases. In general these errors are difficult to estimate and vary from system to system. No corrections were made to account for validation bias. Velocity bias results from the greater likelihood of high velocity particles moving through the measurement volume during a given sampling period. The present measurements were burst transit time weighted to correct for velocity bias, as presented in Buchhave *et al.*<sup>27</sup> Velocity gradient bias is due to velocity variation across the measurement volume. These bias errors only become significant very near the wall, and in the present study these were quite small, and therefore, no velocity gradient bias corrections were made. Bias estimates were combined with the precision uncertainties to calculate the overall uncertainties for the measured quantities, as listed with the figures of the reduced data.

Two methods were used to determine the friction velocity,  $u_\tau$ , for both the smooth and rough surfaces, as listed in Table I. The first was the total stress method, which assumes that a nominally constant shear stress region exists in the inner part of the boundary layer which is equal to the wall shear stress. The total stress was calculated at the plateau of the Reynolds shear stress profile in the overlap region of the boundary layer by summing the contributions of the viscous and turbulent stresses. For the smooth wall, the friction velocity was also determined using the Clauser<sup>28</sup> chart method, with log-law constants  $\kappa=0.41$  and  $B=5.0$ . A modified Clauser chart method was also employed to determine the friction velocity on the rough wall.<sup>14,17</sup> This method also solves for the error in origin, or wall offset due to roughness, as listed in Table I. The friction velocity values obtained using the Clauser (smooth) and modified Clauser (rough) methods are used in the subsequent data reduction; however, using  $u_\tau$  determined from the total stress method would not change the trends in the presented results since the values obtained from both methods show good agreement. The uncertainty in  $u_\tau$  for the smooth walls using the Clauser chart method is  $\pm 3\%$ , and the uncertainty in  $u_\tau$  for the rough walls using the modified Clauser chart method was  $\pm 5\%$ . The un-

certainty in  $u_\tau$  using the total stress method is  $\pm 7\%$  for both the smooth and rough walls.

The boundary layer parameters  $\delta$ ,  $\delta^+$ ,  $\delta^*$ , and  $\theta$  for the smooth and rough walls are listed in Table I. The physical growth of the boundary layer was significantly higher on the rough walls, with the displacement and momentum thicknesses more than doubling for the roughest surface as compared to the smooth wall for the same freestream velocity. For this study,  $\delta$  is taken as the wall normal location where the mean velocity is 99.5% of the freestream velocity. The values  $\delta^*$  and  $\theta$  were calculated assuming a linear velocity profile from the data point closest to the wall and  $y=0$  for the smooth surface. For the rough surfaces, a logarithmic velocity profile from the data point closest to the wall and  $y=0$  was assumed.

### III. RESULTS AND DISCUSSION

#### A. Mean flow

Mean velocity profiles for the seven surfaces plotted in inner variables are shown in Fig. 2. The smooth wall results of DeGraaff and Eaton<sup>29</sup> taken at  $Re_\theta=5200$  are shown for comparison. Both types of rough surfaces display a linear-

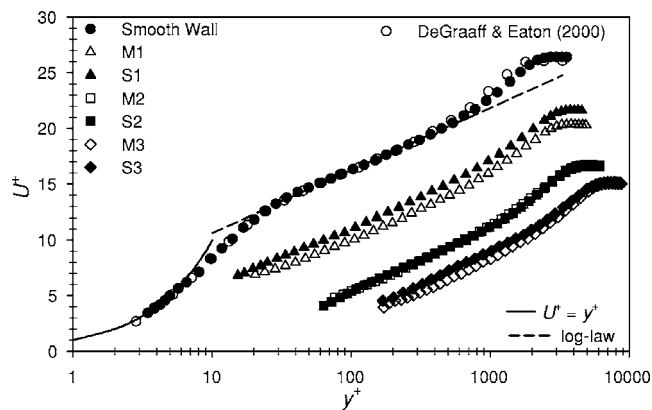


FIG. 2. Mean velocity profiles for all surfaces in inner variables.  $U^+ \pm 3\%$  for smooth wall and  $\pm 5\%$  for rough walls.

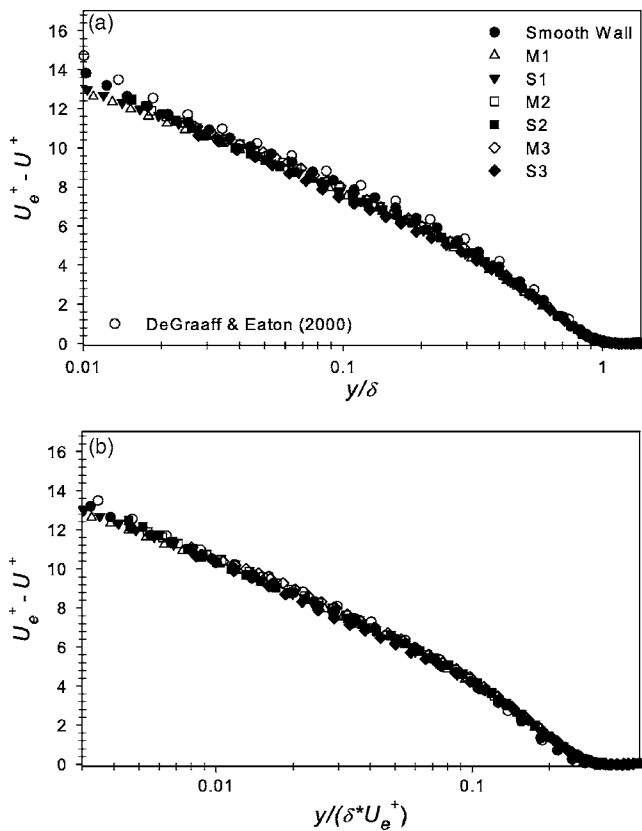


FIG. 3. Mean velocity profiles in velocity defect form for all surfaces: (a) classic scaling; (b) Rotta-Clauser scaling.  $(U_e - U)/U_\tau \pm 3\%$  for smooth wall and  $\pm 5\%$  for rough walls.

log region that is shifted by the roughness function,  $\Delta U^+$ , below the smooth profile, indicating an increased momentum deficit on these surfaces. The sandgrain and mesh surface produced roughness functions range from  $\Delta U^+ = 5.2$  to 13.7, as listed in Table I. It is of note that similar roughness functions are obtained for the mesh and sandgrain surfaces at nominally the same unit Reynolds number even though the roughness heights,  $k$ , differ substantially. This is most evident for the 80-grit sandpaper and fine mesh. The mesh produces a roughness function 20% larger than the sandpaper although the roughness height of the sandpaper is more than twice that of the mesh. The equivalent sand roughness height,  $k_s$ , defined as the uniform sand roughness height that gives that same roughness function in the fully rough regime,<sup>30</sup> is also listed in Table I.  $k_s$  provides a common measure of the influence of the roughness on the mean flow and is related to  $\Delta U^+$  as shown in the following:

$$\Delta U^+ = \frac{1}{\kappa} \ln(k_s^+) + B - C, \quad (2)$$

where  $C$  is the roughness function intercept for uniform sand roughness equal to 8.5.

The mean velocity profiles for all test cases are presented in velocity-defect form in Fig. 3. Again, shown for comparison are the smooth wall results of DeGraaff and Eaton.<sup>30</sup> Figure 3(a) shows the results using classic outer scaling with normalization by  $u_\tau$  and  $\delta$ . Excellent collapse of the present smooth and rough wall results is seen in the outer

part of the boundary layer. The collapse is slightly improved using the Rotta-Clauser length scale ( $\delta^+ U_e^+$ ), as shown in Fig. 3(b). These results indicate that the outer layer mean flow is largely insensitive to surface condition. Further discussion of the mean flow profiles and velocity-defect scaling for the present surfaces is found in Connelly *et al.*<sup>31</sup>

## B. Reynolds stresses and quadrant analysis

The Reynolds stress profiles for the rough and smooth surfaces will now be presented. Ideally, the Kármán number ( $\delta^+$ ) should be matched to investigate outer layer similarity between smooth and rough surfaces. If the disparity between the smooth and rough wall Kármán number is too large it would be difficult to discern if changes in the profiles in the outer layer are due to roughness or Reynolds number effects. It has been shown that the profiles of streamwise Reynolds normal stress,  $\overline{u'^2}$ , exhibit an increasing peak in the buffer layer (at  $y^+ \approx 15$ ) with increasing Kármán number for smooth wall flows.<sup>29</sup> A more slowly rising log-layer plateau in  $\overline{u'^2}$  has also been noted in the studies of DeGraaff and Eaton<sup>29</sup> and Fernholz and Finley<sup>32</sup> for boundary layers, and Morrison *et al.*<sup>33</sup> for fully developed pipe flow. Figure 4 shows smooth wall Reynolds stress profiles for a range of  $\delta^+$  similar to that covered in this study. Included in this graph are the smooth wall results from the current study ( $\delta^+ = 2480$ ), a higher Kármán number smooth wall case obtained in the same facility<sup>17</sup> ( $\delta^+ = 5170$ ), and the smooth wall results of DeGraaff and Eaton<sup>29</sup> ( $\delta^+ = 1780$  and 4570). It should be noted that the apparent differences observed in all the Reynolds stresses in the near-wall region ( $y/\delta < 0.03$ ) are primarily due to the use of outer scaling. There is a slight increase in the log-layer plateau for the streamwise normal Reynolds stress with increasing Kármán number [Fig. 4(a)] at  $0.03 < y/\delta < 0.1$ . Significant differences are not observed in  $\overline{u'^2}$  for  $y/\delta > 0.1$ . Reasonable agreement is observed for  $\overline{v'^2}$  and  $-\overline{u'v'}$  in the overlap and outer layer. There do not appear to be any definitive trends in these Reynolds stresses with increasing Kármán number in agreement with the conclusions of DeGraaff and Eaton.<sup>29</sup> The Kármán-number-dependent differences in the Reynolds stresses in the overlap and outer flow are only observed in  $\overline{u'^2}$  and are small (well within the experimental uncertainty). Therefore, subsequent comparisons of the rough wall profiles will be made to the present smooth wall profiles at  $\delta^+ = 2480$ .

Figures 5–7 show the Reynolds normalized Reynolds stress profiles ( $\overline{u'^2}$ ,  $\overline{v'^2}$ , and  $-\overline{u'v'}$ ) for the smooth and rough walls. In the first graph (a), all the surfaces are presented together, along with the smooth wall results of DeGraaff and Eaton,<sup>29</sup> at  $Re_\theta = 5200$  ( $\delta^+ = 1780$ ), for comparison. Additionally, smooth and rough wall results are shown in log scaling to highlight the approximate location where the profiles diverge. The lines on Figs. 5–7 represent  $5k/\delta$  (solid line) and  $3k_s/\delta$  (dashed line) for each of the rough surfaces, with endpoint symbols identifying the type of surface. Five roughness heights<sup>4</sup> and/or three equivalent sandgrain roughness heights<sup>8</sup> have previously been identified as potential wall-normal limits of the roughness sublayer.

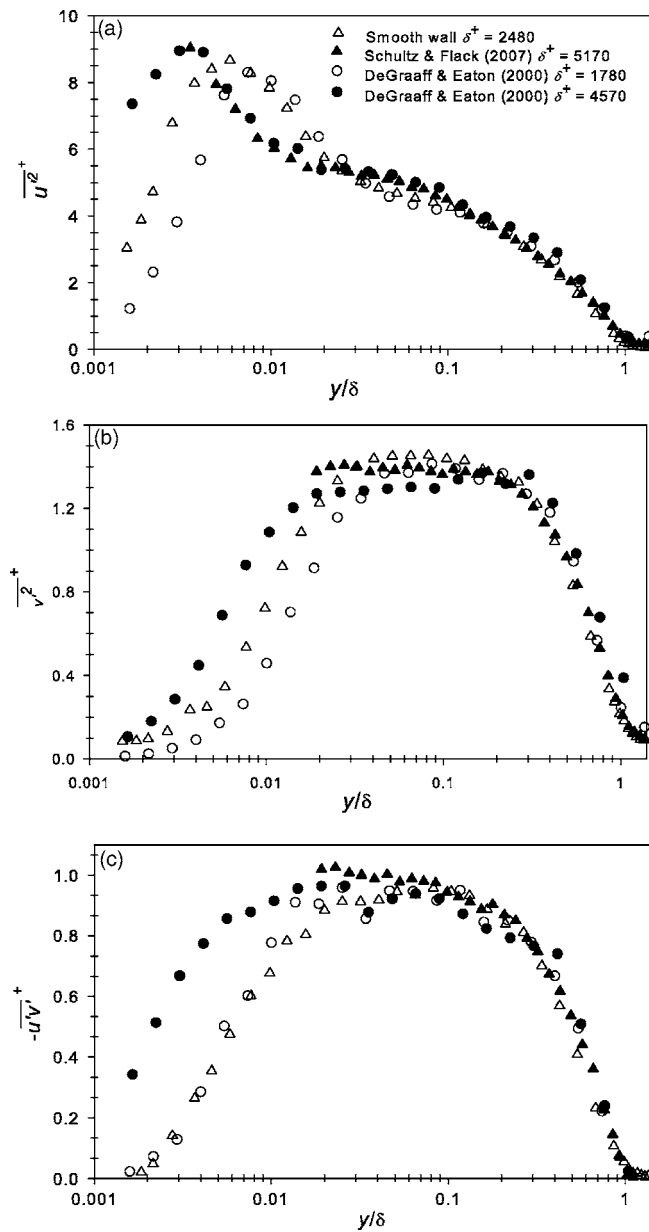


FIG. 4. Smooth wall Reynolds stress profiles in outer variables for a range of  $\delta^+$ : (a)  $\overline{u'^2}^+$ ; (b)  $\overline{v'^2}^+$ ; (c)  $-\overline{u'v'}^+$ . Symbols listed in (a).

The streamwise Reynolds normal stresses,  $\overline{u'^2}^+$  (Fig. 5) for the smooth and rough walls show excellent agreement throughout the outer region of the boundary layer. Outer layer similarity of  $\overline{u'^2}^+$  has been observed in numerous other studies of rough wall boundary layers, as discussed in the review articles of Raupach *et al.*<sup>4</sup> and Jiménez.<sup>1</sup> Near the wall ( $y/\delta \leq 0.04$ ),  $\overline{u'^2}^+$  is significantly lower on the rough walls. For the mildest roughness (M1, S1), this corresponds to  $y^+ \approx 120-13$ , near the location of the outer edge of the buffer layer in a smooth wall flow. The suppression of  $\overline{u'^2}^+$  increases with increasing roughness Reynolds number for flows in the transitionally rough regime. For flows in the fully rough regime, the near-wall peak in  $\overline{u'^2}^+$  is absent entirely. Ligrani and Moffat<sup>13</sup> identified the absence of a near-wall peak in  $\overline{u'^2}^+$  as an indicator of fully rough flow. Flores

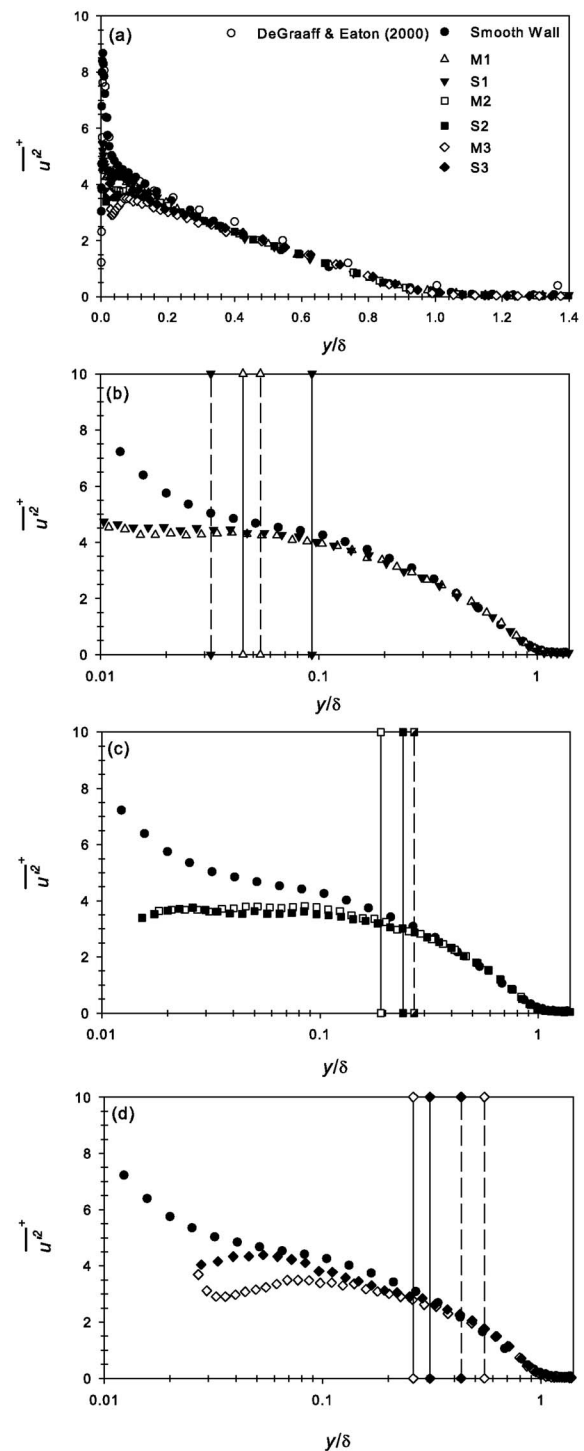


FIG. 5. Streamwise Reynolds normal stress profiles in outer variables: (a) all profiles; (b) smooth, M1 and S1; (c) smooth, M2, and S2; (d) smooth, M3, and S3. (—)  $5k/\delta$ ; (---)  $3k_s/\delta$ ; uncertainty in  $\overline{u'^2}^+ \pm 8\%$ . Symbols listed in (a).

and Jiménez<sup>34</sup> elucidated the physical reasons for this observation identifying that the low-speed streaks and quasi-streamwise vortices of the buffer layer are shortened in rough wall flows. This, in turn, results in decreased streamwise velocity fluctuations. For fully rough flows, surface roughness eliminates near-wall viscous effects, necessarily altering the entire viscous sublayer. Therefore, the likely

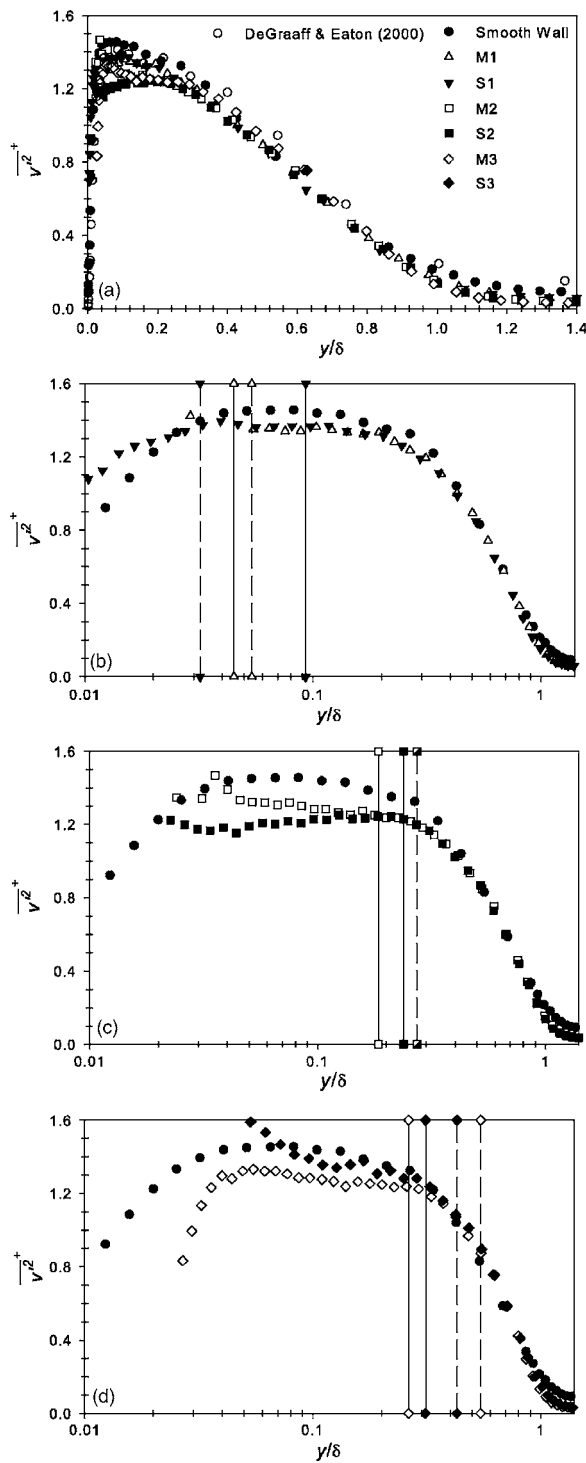


FIG. 6. Wall-normal Reynolds normal stress profiles in outer variables: (a) all profiles; (b) smooth, M1, and S1; (c) smooth, M2, and S2; (d) smooth, M3, and S3. (—)  $5k/\delta$ ; (---)  $3k_s/\delta$ ; uncertainty in  $\overline{v'^2} \pm 9\%$ . Symbols listed in (a).

minimum wall-normal extent of roughness influence for fully rough flows is the location of the inner limit of the log-law region, even for small roughness heights.

The wall-normal Reynolds normal stresses,  $\overline{v'^2}$  (Fig. 6) also indicate good collapse in the outer region of the boundary layer. This result is in agreement with a number of studies.<sup>6-8,13,14</sup> In contrast, the studies of Krogstad *et al.*<sup>9</sup> and

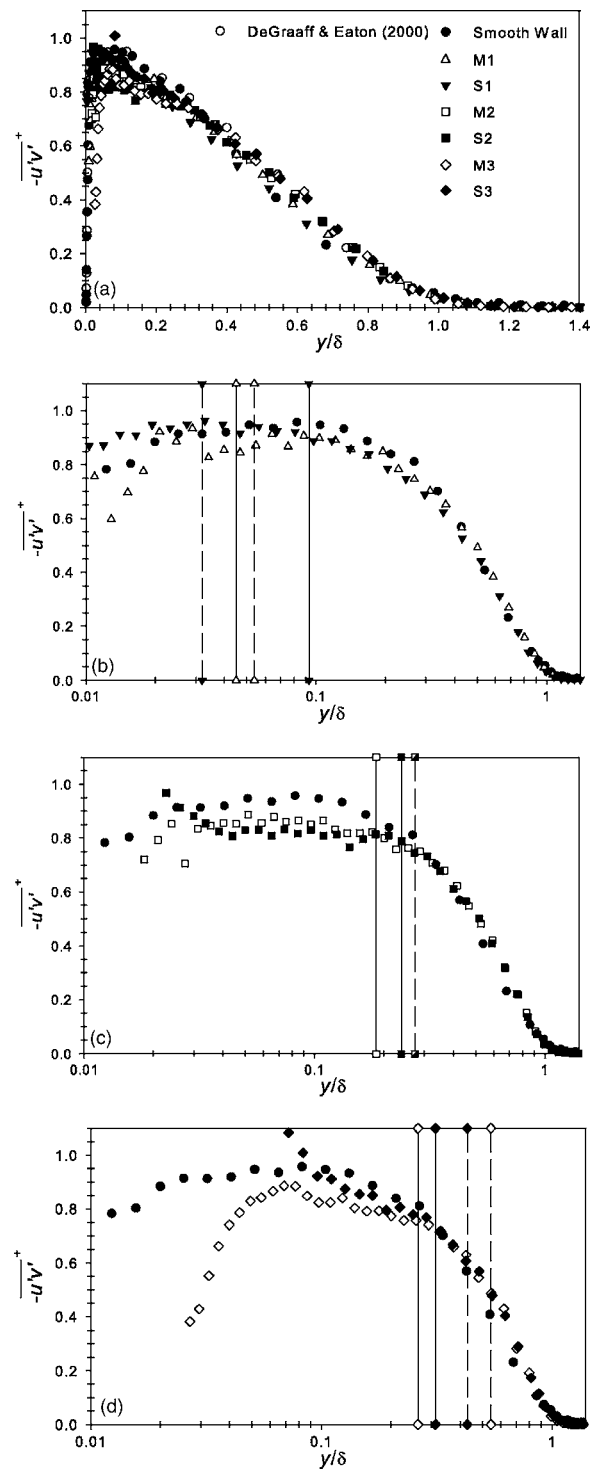


FIG. 7. Reynolds shear stress profiles in outer variables: (a) all profiles; (b) smooth, M1, and S1; (c) smooth, M2, and S2; (d) smooth, M3, and S3. (—)  $5k/\delta$ ; (---)  $3k_s/\delta$ ; uncertainty in  $-\overline{u'v'} \pm 9\%$ . Symbols listed in (a).

Keirsbulck *et al.*<sup>10</sup> showed that significant increases in the wall-normal Reynolds normal stress penetrate well into the outer layer over rough walls. These findings indicated that there may be a critical roughness height where wall similarity fails, prompting the systematic increase of roughness height in the present study. The roughness in the Krogstad

*et al.*<sup>9</sup> and Keirsbulck *et al.*<sup>10</sup> studies had  $\delta/k_s=15$  and 7, respectively; values similar to the larger mesh and sandpaper roughness of the present study.

The normalized Reynolds shear stress ( $-\overline{u'v'}^+$ ) profiles are presented in Fig. 7. Good collapse of the rough and smooth profiles is again observed in the outer region of the boundary layer outside of a roughness sublayer. While near-wall roughness effects are present for all the Reynolds stresses, similarity exists between rough and smooth walls in the outer layer, outside of the roughness sublayer. The agreement of the  $\overline{v'^2}$  and  $-\overline{u'v'}^+$  profiles supports the concept of universal active motions in the outer layer, where the active motions are the turbulent motions that contribute to the Reynolds shear stress.

The present results are consistent with previous research that has shown similarity outside a roughness sublayer extending  $5k$  or  $3k_s$  from the wall. As observed in Figs. 5–7, the Reynolds stresses show good collapse with smooth wall results for  $y \geq 5k$  or  $y \geq 3k_s$ . For the roughest surfaces (M3, S3),  $5k$  and  $3k_s$  seem to overpredict the region of roughness influence, with a better estimate being  $2k$  or  $1k_s$ . For the moderate (M2, S2) and mild roughness (M1, S1),  $5k$  and  $3k_s$  appear to be appropriate.

Changes in turbulence structure between rough and smooth walls are investigated using standard quadrant decomposition techniques, as described in Wallace *et al.*<sup>35</sup> using hyperbolic hole size,<sup>36</sup>  $H$ , in the trigger function. The contribution to  $\overline{u'v'}$  from a given quadrant,  $Q$ , can be expressed as

$$(\overline{u'v'})_Q = \lim_{T \rightarrow \infty} \frac{1}{T} \int_0^T u'v'(t) I_Q(t) dt, \quad (3)$$

where  $I_Q(t)$  is a trigger function defined as

$$I_Q = \begin{cases} 1 & \text{when } |u'v'|_Q \geq H(\overline{u'^2})^{1/2}(\overline{v'^2})^{1/2} \\ 0 & \text{otherwise.} \end{cases} \quad (4)$$

Figure 8 shows the contributions to the conditionally averaged Reynolds shear stress for all surfaces for the case with a hyperbolic hole size  $H=0$  and identifying stronger events with  $H=2$ . For  $H=0$  there is excellent collapse in the outer layer between the rough and smooth surfaces. When stronger events are identified using  $H=2$ , again the similarity between rough and smooth walls is within the uncertainty of the measurement, with more near-wall scatter for the ejection events (Q2). Krogstad *et al.*<sup>9</sup> observed greater contributions to the Reynolds shear stress from the Q2 and Q4 quadrants for a rough wall covered with a similar mesh surface ( $\delta/k_s=15$ ) as compared to a smooth wall. Outer layer collapse was observed for the Q4 events when the strongest sweeps were identified with a hyperbolic hole size of  $H=4$ . Schultz and Flack<sup>7</sup> observed stronger Q4 and Q2 events near the wall for flow over a packed sphere bed, due to the less strict boundary condition for a rough wall. The contributions from the ejection and sweep events collapsed with the smooth wall profiles in the outer layer. Similar results were noted by Flack *et al.*<sup>8</sup> with outer layer similarity for Q2 and Q4 events.

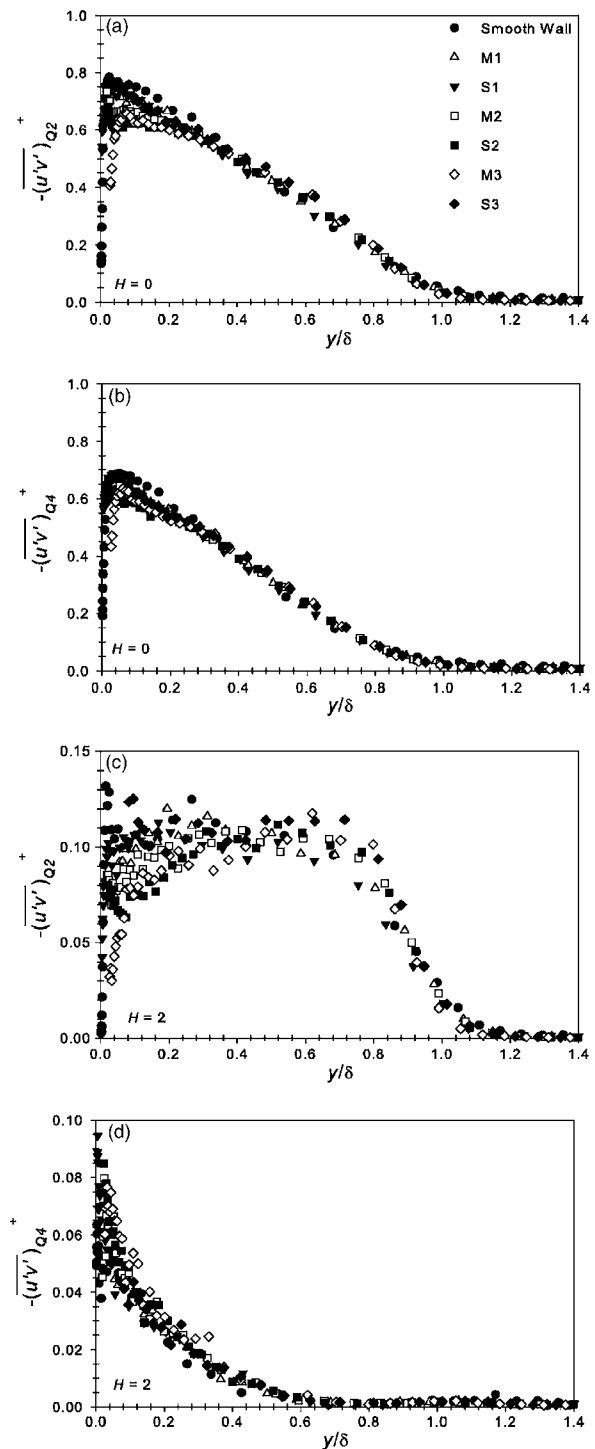


FIG. 8. Contribution to conditionally averaged Reynolds shear stress for all surfaces in outer scaling: (a) Q2 events,  $H=0$ ; (b) Q4 events,  $H=0$ ; (c) Q2 events,  $H=2$ ; (d) Q4 events,  $H=2$ .

### C. Velocity triple products and higher order moments

The distributions of the normalized triple products  $\overline{u'^3}^+$  and  $\overline{v'^3}$ , as well as the normalized axial and wall-normal turbulent flux of the Reynolds shear stress,  $\overline{u'^2v'}^+$  and  $\overline{u'v'^2}$ , are shown in Fig. 9. Andreopoulos and Bradshaw<sup>37</sup> pointed out that the velocity triple products are very sensitive to changes in surface condition. However, due to their inher-



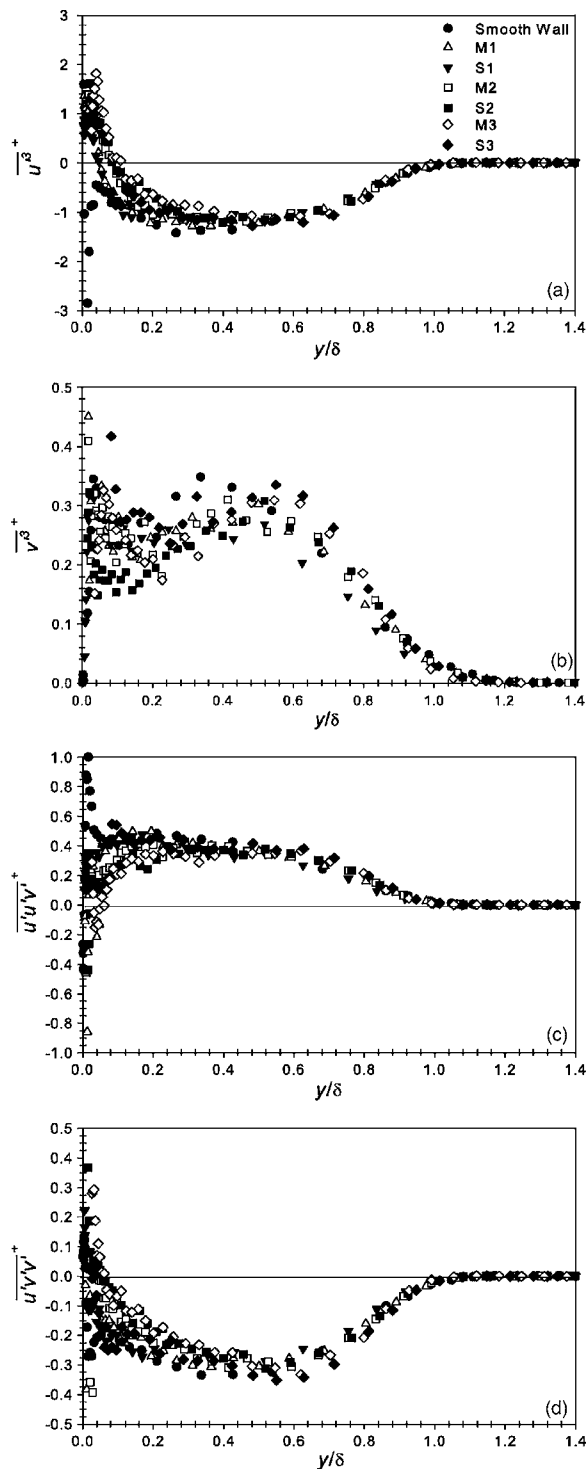


FIG. 9. Velocity triple products for all surfaces in outer scaling: (a)  $\overline{u^3}^+$ ; (b)  $\overline{v^3}^+$ ; (c)  $\overline{u'u'v'}^+$ ; (d)  $\overline{u'v'v'}^+$ . Uncertainty in  $\overline{u^3}^+ \pm 16\%$ ,  $\overline{v^3}^+ \pm 25\%$ ,  $\overline{u'^2v'}^+ \pm 17\%$ ,  $\overline{u'v'^2}^+ \pm 19\%$ .

ently high experimental uncertainty, it is difficult to use them to draw definitive conclusions with regard to the extent of the roughness influence. That notwithstanding, all of the higher order moments display similarity within measurement uncertainty for  $y > 5k$  and  $y > 3k_s$ . Differences in rough and smooth wall profiles are present in the near-wall region. As

indicated in Fig. 9(a),  $\overline{u^3}^+$  for the rough surfaces is positive in the near-wall region, becoming negative in the outer layer. The smooth wall remains negative across the entire boundary layer. A difference between rough and smooth walls in the distribution  $\overline{u^3}^+$  is not surprising considering the destruction of the near-wall peak that is present in the profiles of  $\overline{u'^2}^+$  for a rough surface. Structural differences, including the breakup of streamwise vortices on rough walls,<sup>34</sup> change the mechanics of momentum transfer near the wall. Outer layer agreement in  $\overline{u^3}^+$  between the profiles for rough and smooth walls has also been observed by Andreopoulos and Bradshaw,<sup>37</sup> Bandyopadhyay and Watson,<sup>38</sup> Schultz and Flack,<sup>7</sup> and Flack *et al.*<sup>8</sup>

The aforementioned experimental uncertainty makes it difficult to draw a conclusion regarding the near-wall behavior of  $\overline{v^3}^+$ . The smooth wall profiles lie within the bounds of the rough surface profiles near the wall. Significant differences in  $\overline{v^3}^+$  have been observed for two-dimensional roughness.<sup>5,38</sup> The mesh roughness of Antonia and Krogstad<sup>5</sup> also differed from the smooth wall for  $\overline{v^3}^+$ , however, the difference was not as dramatic as the transverse rod roughness, and the shape of the profile was similar to the smooth wall in the outer layer. Schultz and Flack<sup>7</sup> noted differences in  $\overline{v^3}^+$  out to  $8k$  for flow over a packed bed of spheres, while Flack *et al.*<sup>8</sup> observed differences in the triple products only out to  $5k$  or  $3k_s$  for milder sandgrain and mesh roughness.

The normalized axial and wall-normal turbulent flux of the Reynolds shear stress,  $\overline{u'^2v'}$  and  $\overline{u'v'^2}$ , also demonstrate outer layer similarity as indicated in Figs. 9(c) and 9(d). Antonia and Krogstad<sup>5</sup> show significant changes in  $\overline{u'^2v'}$  in the outer layer for the flow over the rods, but similar shaped profiles and near collapse for the mesh roughness. Andreopoulos and Bradshaw<sup>37</sup> noted that the general shapes of the  $\overline{u'^2v'}$  and  $\overline{u'v'^2}$  profiles in the outer layer were the same for rough and smooth walls, while near-wall differences, including a change in sign, were observed within  $10k$ . They concluded that the near-wall changes in the triple products were associated with strong sweeps near the surface of a rough wall.

#### IV. CONCLUSIONS

These results provide support for Townsend's Reynolds number similarity hypothesis for uniform three-dimensional roughness in flows, where  $k$  and  $k_s$  are a significant fraction of  $\delta$ . Based upon these findings, even comparatively large roughness elements that have a significant effect on the mean flow, can be considered a small perturbation to the boundary layer with regards to the outer layer. While previous results have shown outer layer differences between smooth and rough walls, the present results show that the roughness influence in the outer layer is not observed for  $\delta/k \geq 19$  or  $\delta/k_s \geq 5.5$ . While one would be tempted to test larger roughness elements, obtaining smaller values of  $\delta/k$  is difficult in a boundary layer, which has been given sufficient development region for the velocity-defect profiles to achieve streamwise self-similarity. As the roughness height increases,

the growth rate of the boundary layer increases as well, limiting the ratio of  $\delta/k$ , which can be generated. In developing boundary layers or flows with a fixed outer scale (e.g., pipes and channels), much smaller values of  $\delta/k$  may be obtained. In these cases, changes in the outer layer turbulence may be expected to occur as at some point as the flow must no longer retain the character of a wall-bounded shear flow, becoming dominated by bluff body wakes. For boundary layers that have reached self-similarity, there does not appear to be a critical roughness height that produces modifications to the turbulence that are observed throughout all or most of the boundary layer. Instead, the outer flow is only gradually modified with increasing roughness height as the roughness sublayer, extending  $5k$  or  $3k_s$  from the wall, begins to occupy an ever increasing fraction of the outer layer.

## ACKNOWLEDGMENTS

The authors would like to thank the Office of Naval Research for providing the financial support under Grants Nos. N00014-06-WR20069 and N00014-06-WR20218, and the United States Naval Academy Hydromechanics Laboratory for providing technical support.

- <sup>1</sup>J. Jiménez, "Turbulent flows over rough walls," *Annu. Rev. Fluid Mech.* **36**, 173 (2004).
- <sup>2</sup>F. R. Hama, "Boundary-layer characteristics for rough and smooth surfaces," *Trans. SNAME* **62**, 333 (1954).
- <sup>3</sup>P. R. Bandyopadhyay, "Rough-wall turbulent boundary layers in the transition regime," *J. Fluid Mech.* **180**, 231 (1987).
- <sup>4</sup>M. R. Raupach, R. A. Antonia, and S. Rajagopalan, "Rough-wall boundary layers," *Appl. Mech. Rev.* **44**, 1 (1991).
- <sup>5</sup>R. A. Antonia and P.-Å. Krogstad, "Turbulence structure in boundary layers over different types of surface roughness," *Fluid Dyn. Res.* **28**, 139 (2001).
- <sup>6</sup>M. P. Schultz and K. A. Flack, "Turbulent boundary layers over surfaces smoothed by sanding," *J. Fluids Eng.* **125**, 863 (2003).
- <sup>7</sup>M. P. Schultz and K. A. Flack, "Outer layer similarity in fully rough turbulent boundary layers," *Exp. Fluids* **38**, 328 (2005).
- <sup>8</sup>K. A. Flack, M. P. Schultz, and T. A. Shapiro, "Experimental support for Townsend's Reynolds number similarity hypothesis on rough walls," *Phys. Fluids* **17**, 035102 (2005).
- <sup>9</sup>P.-Å. Krogstad, R. A. Antonia, and L. W. B. Browne, "Comparison between rough- and smooth-wall turbulent boundary layers," *J. Fluid Mech.* **245**, 599 (1992).
- <sup>10</sup>L. Keirsbulck, L. Labraga, A. Mazouz, and C. Tournier, "Surface roughness effects on turbulent boundary layer structures," *J. Fluids Eng.* **124**, 127 (2002).
- <sup>11</sup>A. A. Townsend, *The Structure of Turbulent Shear Flow*, 2nd ed. (Cambridge University Press, Cambridge, UK, 1976).
- <sup>12</sup>A. E. Perry and M. S. Chong, "On the mechanism of wall turbulence," *J. Fluid Mech.* **119**, 173 (1982).
- <sup>13</sup>P. M. Ligrani and R. J. Moffat, "Structure of transitionally rough and fully rough turbulent boundary layers," *J. Fluid Mech.* **162**, 69 (1986).
- <sup>14</sup>A. E. Perry and J. D. Li, "Experimental support for the attached-eddy hypothesis in zero-pressure gradient turbulent boundary layers," *J. Fluid Mech.* **218**, 405 (1990).
- <sup>15</sup>G. J. Kunkel and I. Marusic, "Study of the near-wall-turbulent region of the high-Reynolds-number boundary layer using an atmospheric flow," *J. Fluid Mech.* **548**, 375 (2006).
- <sup>16</sup>M. A. Shockling, J. J. Allen, and A. J. Smits, "Roughness effects in turbulent pipe flow," *J. Fluid Mech.* **564**, 267 (2006).
- <sup>17</sup>M. P. Schultz and K. A. Flack, "The rough-wall turbulent boundary layer from the hydraulically smooth to the fully rough regime," *J. Fluid Mech.* **580**, 381 (2007).
- <sup>18</sup>P.-Å. Krogstad and R. A. Antonia, "Surface roughness effects in turbulent boundary layers," *Exp. Fluids* **27**, 450 (1999).
- <sup>19</sup>M. F. Tachie, D. J. Bergstrom, and R. Balachandar, "Rough wall turbulent boundary layers in shallow open channel flow," *J. Fluids Eng.* **122**, 533 (2000).
- <sup>20</sup>S. Leonardi, P. Orlandi, R. J. Smalley, L. Djenidi, and R. A. Antonia, "Direct numerical simulations of turbulent channel flow with transverse square bars on one wall," *J. Fluid Mech.* **491**, 229 (2003).
- <sup>21</sup>K. Bhaganagar, J. Kim, and G. Coleman, "Effect of roughness on wall-bounded turbulence," *Trans. Inst. Chem. Eng., Part A* **72**, 463 (2004).
- <sup>22</sup>H. Schlichting, *Boundary-layer Theory*, 7th ed. (McGraw-Hill, New York, 1979).
- <sup>23</sup>P. Bradshaw, "A note on 'critical roughness height' and 'transitional roughness'," *Phys. Fluids* **12**, 1611 (2000).
- <sup>24</sup>R. J. Adrian, "Laser velocimetry," in *Fluid Mechanics Measurements*, 2nd ed. edited by R. J. Goldstein (Taylor and Francis, Washington, DC., 1996).
- <sup>25</sup>R. J. Moffat, "Describing the uncertainties in experimental results," *Exp. Therm. Fluid Sci.* **1**, 3 (1988).
- <sup>26</sup>R. V. Edwards, "Report of the special panel on statistical particle bias problems in laser anemometry," *J. Fluids Eng.* **109**, 89 (1987).
- <sup>27</sup>P. Buchhave, W. K. George, and J. L. Lumley, "The measurements of turbulence with the laser-Doppler anemometer," *Annu. Rev. Fluid Mech.* **11**, 443 (1970).
- <sup>28</sup>F. H. Clauser, "Turbulent boundary layers in adverse pressure gradients," *J. Aeronaut. Sci.* **21**, 91 (1954).
- <sup>29</sup>D. B. DeGraaff and J. K. Eaton, "Reynolds-number scaling of the flat-plate turbulent boundary layer," *J. Fluid Mech.* **422**, 319 (2000).
- <sup>30</sup>J. Nikuradse, "Laws of flow in rough pipes," *NASA Tech. Memo.* **1292**, 1, (1933).
- <sup>31</sup>J. S. Connelly, M. P. Schultz, and K. A. Flack, "Velocity defect scaling for turbulent boundary layers with a range of relative roughness," *Exp. Fluids* **40**, 188 (2006).
- <sup>32</sup>H. H. Fernholz and P. J. Finley, "Incompressible zero-pressure-gradient turbulent boundary layer: An assessment of the data," *Prog. Aerosp. Sci.* **32**, 245 (1996).
- <sup>33</sup>J. F. Morrison, B. J. McKeon, W. Jiang, and A. J. Smits, "Scaling of the streamwise velocity component in turbulent pipe flow," *J. Fluid Mech.* **508**, 99 (2004).
- <sup>34</sup>O. Flores and J. Jiménez, "Effect of wall-boundary disturbances on turbulent channel flows," *J. Fluid Mech.* **566**, 357 (2006).
- <sup>35</sup>J. M. Wallace, H. Eckelmann, and R. S. Brodkey, "The wall region in turbulent shear flow," *J. Fluid Mech.* **54**, 39 (1972).
- <sup>36</sup>S. S. Lu and W. W. Willmarth, "Measurements of the structure of the Reynolds stress in a turbulent boundary layer," *J. Fluid Mech.* **60**, 481 (1973).
- <sup>37</sup>J. Andreopoulos and P. Bradshaw, "Measurements of turbulence structure in the boundary layer on a rough surface," *Boundary-Layer Meteorol.* **20**, 201 (1981).
- <sup>38</sup>P. R. Bandyopadhyay and R. D. Watson, "Structure of rough-wall boundary layers," *Phys. Fluids* **31**, 1877 (1988).